BBA - Bioenergetics 1861 (2020) 148301

Contents lists available at ScienceDirect

BBA - Bioenergetics

journal homepage: www.elsevier.com/locate/bbabio

D1-S169A substitution of photosystem II reveals a novel S_2-state structure

Ipsita Ghosh[a,1], Gourab Banerjee[a,1], Krystle Reiss[a], Christopher J. Kim[b], Richard J. Debus[b,*], Victor S. Batista[a], Gary W. Brudvig[a,*]

[a] Department of Chemistry, Yale University, New Haven, CT 06520-8107, USA
[b] Department of Biochemistry, University of California, Riverside, CA 92521, USA

ARTICLE INFO

Keywords:
Cyanobacteria
Decay kinetics
Mutation
Oxygen evolution
Photosystem II
Structure

ABSTRACT

In photosystem II (PSII), photosynthetic water oxidation occurs at the O_2-evolving complex (OEC), a tetra-manganese-calcium cluster that cycles through light-induced redox intermediates (S_0–S_4) to produce oxygen from two substrate water molecules. The OEC is surrounded by a hydrogen-bonded network of amino-acid residues that plays a crucial role in proton transfer and substrate water delivery. Previously, we found that D1-S169 was crucial for water oxidation and its mutation to alanine perturbed the hydrogen-bonding network. In this study, we demonstrate that the activation energy for the S_2 to S_1 transition of D1-S169A PSII is higher than wild-type PSII with a ~1.7–2.7× slower rate of charge recombination with Q_A^- relative to wild-type PSII. Arrhenius analysis of the decay kinetics shows an E_a of 5.87 ± 1.15 kcal mol^{-1} for decay back to the S_1 state, compared to 0.80 ± 0.13 kcal mol^{-1} for the wild-type S_2 state. In addition, we find that ammonia does not affect the S_2-state EPR signal, indicating that ammonia does not bind to the Mn cluster in D1-S169A PSII. Finally, a QM/MM analysis indicates that an additional water molecule binds to the Mn4 ion in place of an oxo ligand O5 in the S_2 state of D1-S169A PSII. The altered S_2 state of D1-S169A PSII provides insight into the $S_2 \rightarrow S_3$ state transition.

1. Introduction

Green plants, cyanobacteria and algae photosynthesize to produce oxygen which is essential for aerobic living organisms. Thus, elucidation of the mechanistic details of water oxidation is critical for understanding one of the key biochemical process in nature, potentially providing insights for design of artificial water-oxidation catalysts [1]. Photosynthetic water oxidation occurs in photosystem II (PSII), which is a transmembrane protein complex comprised of core protein subunits, including D1, D2, CP43 and CP47 and other extrinsic subunits [2–6]. Water oxidation is triggered by photo-induced charge separation between P_{680}, a quartet of chlorophyll molecules and two nearby pheophytin molecules. Charge separation leads to oxidation of a tyrosine, D1-Y161 referred to as Tyr_Z, inducing the cyclic water-oxidation process at the oxygen-evolving complex (OEC) of PSII (Fig. 1) [2–6]. The OEC contains a Mn_4CaO_5 cluster that undergoes single-step oxidations forming the four S-states (S_0–S_3) (Fig. 1B) [7]. The OEC, Tyr_Z, and P_{680} are referred together as the donor side of the PSII. Each S-state turnover is accompanied by the sequential reduction of two quinone electron acceptors, Q_A and Q_B. Q_B accepts two electrons and two protons in response to two successive charge separations to form a plastoquinol molecule that is exchanged with an oxidized quinone from the plastoquinone pool [2–6]. This exchange is the rate-limiting step in the water-oxidation cycle leading to O_2 evolution during the $S_3 \rightarrow S_0$ transition [8].

The efficiency of the S-state cycle is also regulated by the choreographed removal of protons from PSII into the lumen to maintain the proton motive force. The OEC is surrounded by a hydrogen-bonded network of amino-acid residues, waters and inorganic ions that provide conducive proton-transfer pathways. These hydrogen-bonded networks also participate in substrate water delivery and removal of evolved oxygen, and maintain the redox potential of the cluster [6]. Hence, to understand the mechanism of water oxidation, it is important to decipher the role of these amino-acid residues in the S-state transitions.

In recent years, the structures of the individual S_n states have been established by static and serial femtosecond X-ray crystallography, extended X-ray absorption fine structure (EXAFS) spectroscopy, electron paramagnetic resonance (EPR) studies and quantum mechanical studies [13–17]. The S_2 state is generated by continuous illumination of PSII in the S_1 state at 130–200 K or by a single turnover flash at room

* Corresponding authors.
E-mail addresses: richard.debus@ucr.edu (R.J. Debus), gary.brudvig@yale.edu (G.W. Brudvig).
[1] These authors contributed equally.

https://doi.org/10.1016/j.bbabio.2020.148301
Received 18 November 2019; Received in revised form 18 August 2020; Accepted 22 August 2020
Available online 27 August 2020

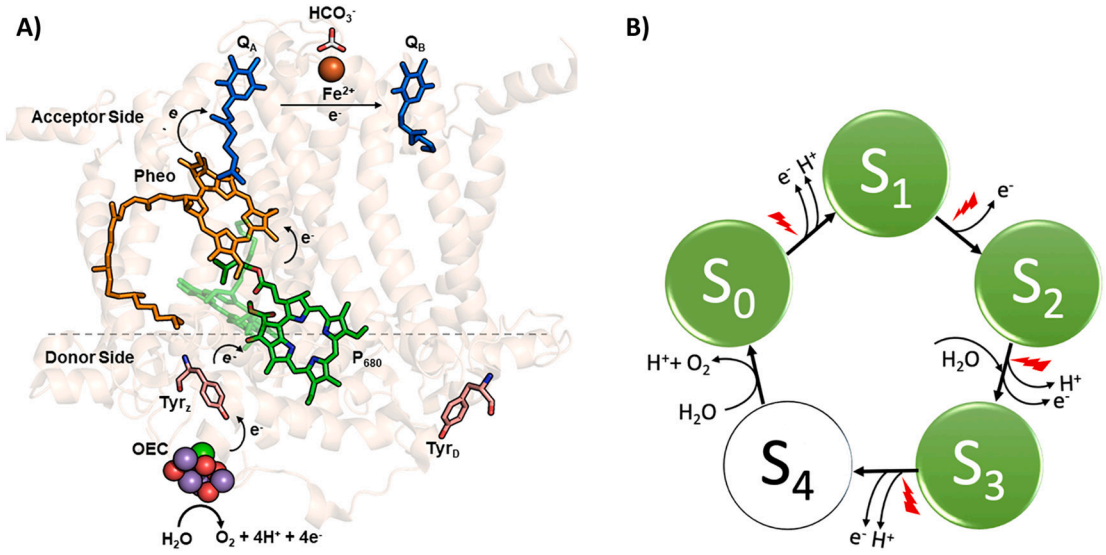

Fig. 1. A) The electron donor and acceptor sides of photosystem II. The donor side contains the Mn_4CaO_5 complex (OEC), where the Mn ions are marked in purple, O in red and Ca in green. The other two components of the donor side include Tyr_Z (a tyrosine molecule in the D1 subunit of PSII, D1-Y161) and P_{680}, which is a group of chlorophyll *a* and pheophytin *a* molecules that function as the primary electron donor. The acceptor side contains a pheophytin molecule (Pheo) which accepts electrons from P_{680}. The electrons are transferred from $Pheo^-$ to the primary quinone electron acceptor Q_A and then to the secondary quinone electron acceptor, Q_B. The Fe^{2+} and HCO_3^- ions on the acceptor side assist in electron transfer from Q_A to Q_B [6,9–11]. The Tyr_D molecule, D2-Y160 (a tyrosine molecule in the D2 subunit of PSII) plays an important role in the oxidation of the S_0 state to the S_1 state [12]. The residues are marked in distinct colors for clarity and follow from the 3WU2 structure [13]. **B)** Schematic representation showing the S-state cycle. This period-four cycle illustrated here involves light-induced single-step oxidation of the intermediates called the S-states (S_0, S_1, S_2, S_3) along with proton egress and substrate water entry during specific transitions. The S_3 to S_0 transition goes through a transient S_4 state leading to the formation of O_2 as shown in the figure.

temperature. Multiple lines of evidence suggest the presence of spin isomerism in the S_2 state resulting in either a S = 5/2 structure, where Mn1 is oxidized from Mn(III) to Mn(IV), or a S = 1/2 structure, where Mn4 is oxidized to the +4-oxidation state. These isomeric forms are characterized by a g = 4.1 EPR signal and a 18–22 multiline EPR signal centered at g = 2, respectively [18]. Both of these signals are observed in spinach PSII whereas in cyanobacterial PSII only the multiline signal is observed except under special circumstances. The intensity of these EPR signals are sensitive to illumination conditions and demonstrate alterations in the presence of single-point mutations of amino-acid residues or small molecules [19]. The formation of the S_3 state is associated with the binding of a water molecule, proton removal and rearrangement of the hydrogen-bonding network [3,5,8,20]. X-ray free-electron laser (XFEL) and EPR studies have provided detailed structural information on the S_3 state, where all four Mn are in the +4-oxidation state [3]; however, the mechanism of its formation is highly debated. One key issue is characterization of the water molecule that binds to the cluster during the S_2 to S_3 transition, which is essential for a detailed understanding of O—O bond formation during the S_3 to S_0 transition.

The abundance of water molecules surrounding the OEC creates difficulty in tracking the substrate waters. Substrate exchange kinetic studies on the Sr-substituted OEC and inorganic model complexes provide information that has helped to identify the possible substrate water molecules [21,22]. Further, the effects of small molecule water analogues like ammonia and methanol have been studied to understand substrate water binding [23–30]. Single point mutation of amino-acid residues surrounding the OEC, including D1-D61A, D1-V185A, D1-Q165A, D1-N87A, D2-K317A and D1-S169A, have been analyzed by using flash-induced oxygen-evolution and FT-IR studies to reveal their role in the binding of substrate waters, proton transport and O—O bond formation [31–37].

In this study, we focus on the D1-S169A mutation of the PSII. Fig. 2 illustrates the hydrogen-bonding network surrounding the D1-S169 residue. Previously, we have shown that the D1-S169A mutation decreases the efficiency of the S-state cycle and slows oxygen formation. Further, we observed an altered multiline EPR signal for the S_2 state of D1-S169A PSII. Based on FT-IR studies, we proposed that these perturbations may arise from a hindrance in either the proton-transfer pathway or the substrate water-delivery pathway, or possbily both [31]. Here, we studied the altered S_2 state observed in D1-S169A PSII in greater detail. EPR studies probing the energetic landscape of the $S_2 \rightarrow S_1$ decay process provide insight into the activation energy and structure of the OEC in D1-S169A PSII. We also studied the effect of ammonia on the EPR spectra of the S_2 state. These studies have been further supported by a 2500 atom QM/MM-optimized model of the S_2 state that provides insight into the functional importance of D1-S169 residue and the mechanism of the $S_2 \rightarrow S_3$ transition.

2. Materials and methods

2.1. Isolation of PSII from wild type and mutant strains of Synechocystis PCC 6803

The His-tagged wild-type and D1-S169A cells, were constructed as described previously [31]. Single colonies were selected for their ability to grow on solid media containing 5 μg/mL kanamycin monosulfate and 20 μg/mL gentamycin sulfate [38]. The cells were propagated in three 10 L carboys as described previously [35] and bubbled with 5% CO_2 in air. The PSII extraction and purification were performed under dim light conditions at 4 °C using a Ni-NTA super flow affinity resin (Qiagen, Valencia, CA) as described previously [39]. The purified PSII core complexes were concentrated to ~1 mg of Chl/mL and stored in a buffer solution containing 1.2 M betaine, 10% (*v*/v) glycerol, 50 mM MES-NaOH (pH 6.0), 20 mM $CaCl_2$, 5 mM $MgCl_2$, 50 mM histidine, 1 mM EDTA, and 0.03% (*w/v*) *n*-dodecyl β-D-maltoside at −80 °C. The oxygen evolution from the PSII core complexes isolated from wild-type *Synechocystis* sp. PCC 6803 is generally ~2000 μmol O_2 (mg of Chl)$^{-1}$ h^{-1}.

2.2. Polarographic oxygen-evolution measurements

Flash-induced O_2 yields of His-tagged wild-type and D1-S169A PSII

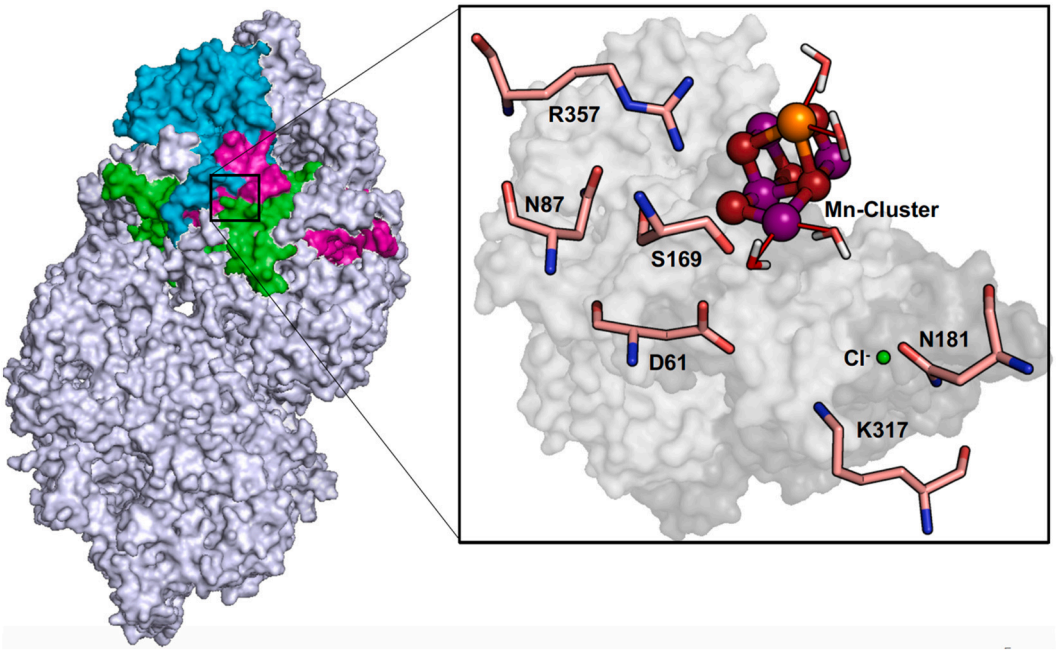

Fig. 2. Photosystem II dimer is shown as a surface structure. Resides in the four major subunits: D1, D2, CP43 and CP47 in one of the monomers are colored. The inset depicts key amino-acid residues in the hydrogen-bonding network around the OEC, chloride and waters. The C atoms are marked in pink, O atoms in red, Mn in purple, N in blue, Ca in orange and Cl^- in green. The figure follows from 3WU2 structure [13].

core complexes were measured using a bare platinum electrode [40]. The samples were suspended in buffer containing 1 M sucrose, 10 mM $CaCl_2$, 200 mM NaCl, and 50 mM MES-NaOH (pH 6.50) as described previously [40]. 500 μM DCBQ and 1 mM K_3FeCN_6 were added as electron acceptors. One flash was provided to generate the S_2 state, followed by a variable delay time. Twenty flashes with an interval spacing of 1 s were then applied and the resulting O_2-yield oscillations were used for analysis of the decay kinetics [40]. The decay kinetics of the S_2 to S_1 state were analyzed by computing the relative population of the S_2 state at the beginning of the 20-flash sequence using the VZAD model using the BOBYQA nonlinear optimization algorithm [41]. The decay kinetics were determined by fitting the data with an exponential decay equation: $y = y_0 \exp(-k\,x)$, where y_0 is the initial S_2 state population, and k is the decay rate constant, respectively.

2.3. Optical measurements

Transient absorbance changes of $Q_A^{\bullet-}$ at 325 nm (ΔA_{325}) were measured with a modified CARY-14 spectrophotometer (On-Line Instrument Systems, Inc., Bogart, GA) operated in single-beam mode [42,43]. The photomultiplier tube was protected with a Corion Solar Blind filter. Actinic flashes (532 nm, ~ 7 ns fwhm; 25–28 mJ/flash) were provided by a frequency-doubled Q-switched Nd:YAG laser [Surelite I (Continuum, Santa Clara, CA)]. For measurements, PSII core complexes were diluted (12 μg of Chl into 0.6 mL final volume) into a buffer solution containing 1.2 M betaine, 10% (*v*/v) glycerol, 50 mM MES-NaOH (pH 6.0), 20 mM $CaCl_2$, 5 mM $MgCl_2$, and 0.03% (*w*/*v*) *n*-dodecyl *β*-D-maltoside; then DCMU (dissolved in DMSO) was added to 25 μM. The sample temperature was 4 °C. Samples were incubated in darkness for 3.5 min, then subjected to two pre-flashes and nine data acquisition flashes spaced 3.5 min apart. The pre-flashes were applied to ensure the oxidation of Y_D prior to data acquisition. The data of multiple samples were averaged.

2.4. Electron paramagnetic resonance studies

EPR samples were concentrated to ~50 μL using Amicon centrifugal cells. The concentrated samples were washed 3–4 times in a buffer containing 50 mM MES-NaOH (pH 6.0), 1 M sucrose, 20 mM $CaCl_2$, 5 mM $MgCl_2$, 1 mM EDTA, 0.5 mM 2-phenyl-1,4-benzoquinone (PPBQ) and concentrated to 1 mg of Chl/mL. The measurements were performed using a Bruker ELEXSYS E500 spectrometer equipped with a SHQ resonator and an Oxford ESR-900 continuous flow cryostat at 7.5 K. The EPR parameters used for recording the spectra are as follows: microwave frequency, 9.38 GHz; modulation frequency, 100 kHz; modulation amplitude, 19.95 G; microwave power, 5 mW; sweep time, 84 s; conversion time, 41 ms; time constant, 82 ms. Each spectrum is the average of two scans. The dark scan of the EPR samples, concentrated to 1 mg of Chl/mL, corresponding to the S_1 state was initially recorded. Then, the S_2 state was generated by illuminating the sample with a Xe lamp in a 200 K acetone/dry ice bath for 5 min and the spectrum was recorded.

2.4.1. Ammonia binding

Ammonia binding was studied in a buffer containing 1 M sucrose, 45 mM HEPES (pH 7.5), 11 mM $Ca(OH)_2$, 0.5 mM EDTA, 0.5 mM PPBQ and 100 mM NH_4Cl. The S_2 state was generated by illuminating dark-adapted PSII samples at 200 K for 5 min. To investigate ammonia binding to the S_2 state of the OEC, PSII samples were annealed at 258 K in an ethylene glycol-dry ice bath for approximately 1 min and then frozen in liquid nitrogen.

2.4.2. $S_2Q_A^-$ decay kinetic studies

Studies of the kinetics of $S_2Q_A^-$ recombination were carried out with samples containing 0.5 mM DCMU (added from a stock solution of 100 mM in DMSO). The PSII samples were illuminated at 200 K in a dry-ice acetone bath to generate the S_2 state, then incubated in a constant temperature bath containing varying concentrations of equilibrated ethanol/ethylene glycol in the dark for different time intervals. The intensity of the S_2-state multiline EPR signal was then recorded. During incubation, the temperature was continuously monitored using a thermocouple. EPR spectral subtractions and the curve fittings were done using Origin Pro (Fig. S1). The decay kinetics of the S_2-state multiline EPR signal were analyzed by fitting the data with the equation: $y = y_0 \exp(-k\,x)$.

2.5. QM/MM calculations

The QM/MM computational model of the oxygen-evolving complex (OEC) was constructed as described in previous work [15,44]. Residues in the model included those with C_α within 15 Å of the OEC. The two chloride anions and all water molecules whose oxygen atoms fall within this boundary were also included. Cut residues were capped with neutral backbone fragments (ACE/NME) whose position was dictated by the location the neighboring residues.

Residues included in the model are listed as follows, with capping residues only including the backbone atoms and are indicated by (parenthesis):

D1 (chain A): (57)-58-67-(68), (81)-82-91-(92), (107)-108-112-(113), (155)-156-192-(193), (289)-290-298-(299), (323)-324-344:C-terminus; CP43 (chain C): (290)-291-(292), (305)-306-314-(315), (334)-335-337-(338), (341)-342-(343), (350)-351-358-(359), (398)-399-402-(403), (408)-409-413-(414); D2 (chain D): (311)-312-321-(322), (347)-348-352:C-terminus.

The model was optimized as a two-layer QM/MM model using the ONIOM [45] method in the Gaussian16 [46] software suite. The QM layer contained the OEC, surrounding residues (D1-S/A169, D1-D170, D1-E189, D1-H332, D1-E333, D1-D342, CP43-E354, the C-terminus of D1-A344, D1-H337, CP43-R357, and D1-D61), and eleven water molecules. Clipped sidechains were modeled as described previously [47]. The QM layer was calculated at the B3LYP [48,49] level of theory, with the LanL2DZ [50,51] basis set and pseudopotential used for Mn and Ca atoms and 6-31G(d) [52] for all others. The lower MM layer was calculated using the AMBER [53] force field. All atoms were allowed to relax, excluding the capping residues and the chloride and oxygen atoms of waters in the MM layer.

3. Results

3.1. Characterization of the S_2 state in D1-S169A PSII

The cw-EPR spectrum of the S_2 state of D1-S169A PSII exhibits a multiline signal where the average hyperfine line spacing of the multiline signal is reduced from ~87.5 G in wild-type PSII to ~72 G, which suggests subtle alterations to the structure of the OEC [31], as seen previously in D1-H332E PSII [42], D1-D61A PSII [28], ammonia-treated [27–30], Ca-depleted [54,55] and Sr/Ca substituted wild-type PSII [39,56–58]. To further probe the alteration of the S_2 state, we studied the decay kinetics of the S_2 state to the S_1 state using polarographic oxygen measurements and time-resolved optical absorption spectroscopy.

The S_2 state decays to the S_1 state in darkness via charge recombination with electrons from the acceptor-side of the PSII [40,56,59,60]. However, the decay kinetics depend on the stability of the S_2 state and the coordination state of the Mn cluster. The S_2-state decay measured polarographically in PSII core complexes exhibited monophasic kinetics and was fit with a single-phase exponential decay function. This decay reflects the back reaction of the S_2 intermediate to the S_1 state.

We observed that the D1-S169A PSII core complexes exhibited a ~ 2.7-fold slower rate of decay to the S_1 state as compared to the wild-type PSII core complexes (Table 1, Fig. 3).

The S_2 state decay measured optically was determined at 325 nm from the kinetics of $Q_A^{\bullet-}$ decay after a single flash applied in the presence of DCMU [42,43,61]. No more than 10% of PSII reaction centers in purified wild-type PSII core complexes from *Synechocystis* sp. PCC 6803 have their Q_B site functionally occupied by native plastoquinone [75]. Nevertheless, DCMU was included to prevent the oxidation of $Q_A^{\bullet-}$ by any native plastoquinone that might occupy the Q_B site. A concentration of 25 μM DCMU was chosen because this concentration eliminates steady-state O_2 evolution by wild-type PSII core complexes in the presence of 400 μM DCBQ and 1 mM K_3FeCN_6; that is, the rate of O_2 evolution measured in the presence of 25 μM DCMU, 400 μM DCBQ, and 1 mM K_3FeCN_6 is the same as the background rate in wild-type PSII core complexes having no exogenous electron acceptors present.

Table 1
Decay Kinetics of PSII core-complexes measured polarographically: comparison of S_2-to-S_1 decay kinetics in wild-type and D1-S169A PSII core complexes, where k^{-1} represents the decay rate. Data from Fig. 3 were fit with a single-component exponential decay model (See Materials and Methods).

	k^{-1} (s)
Wild-type	33 ± 7
D1-S169A	91 ± 33

Charge recombination between $Q_A^{\bullet-}$ and $Y_Z^{\bullet}$ is too rapid (< 0.2 s) to be observed at the timescale employed in our measurements. Consequently, the kinetics shown in Fig. 4 reflect charge recombination between $Q_A^{\bullet-}$ and the S_2 state [42,43]. Previously, we determined that 60–67% of D1-S169A PSII core complexes contain functional Mn_4Ca clusters [31]. The flash-induced formation of slowly-decaying $Q_A^{\bullet-}$ in D1-S169A is about 61% compared to wild-type. This amplitude correlates well with the fraction of D1-S169A PSII centers containing Mn_4Ca clusters [31]. The decay curves were fit with two exponentially-decaying phases plus a constant. These fits (Table 2) demonstrate that $Q_A^{\bullet-}$ recombines with the S_2 state 1.7–2.0 times more slowly in D1-S169A PSII core complexes compared with wild-type, consistent with the polarographic measurements (within error) and further showing that the D1-S169A substitution stabilizes the S_2 state. Note that no electron acceptors were present in the optical measurements to complete with the S_2 state for the oxidation of $Q_A^{\bullet-}$.

Next, to understand the energetic landscape of the decay of the S_2 state of D1-S169A PSII core complexes, we investigated the S_2 to S_1 state transition using EPR spectroscopy at a number of temperatures. We illuminated the dark-incubated DCMU-treated PSII core complexes at 200 K to generate the $S_2Q_A^-$ state (Scheme 1). The same sample was then incubated at different temperatures ranging from 209 K–261 K to monitor the decay of the S_2-state g = 2 multiline EPR signal (Fig. 5a and b, Fig. S2).

The decay rates for the incubation temperatures were calculated and the Arrhenius equation was then used to calculate the activation energy for conversion of the S_2 state into the S_1 state (Fig. 6). The calculated activation energy for conversion of the S_2 state to the S_1 state in wild-type *Synechocystis* PSII core complexes is 0.80 ± 0.13 kcal mol^{-1}. In contrast, the activation energy for conversion of the S_2 state to the S_1 state in D1-S169A PSII core complex is 5.87 ± 1.15 kcal mol^{-1} (Fig. 6). This confirmed that the $S_2 \rightarrow S_1$ transition in D1-S169A PSII has a higher activation energy than wild-type *Synechocystis* PSII. Fig. 7 is a schematic representation of the energetic landscape for the S_2 to S_1 state transition in wild-type and D1-S169A PSII demonstrating a higher energy of activation for the S_2 to S_1 state transition in the mutated PSII.

In our previous paper, we demonstrated by using FTIR spectroscopy that in D1-S169A PSII core-complexes there are significant alterations in the hydrogen-bonding network around the OEC. However, it is unlikely that the ~7× increase in activation energy of the $S_2 \rightarrow S_1$ transition state in D1-S169A PSII arises primarily due to changes in the hydrogen-bonding network associated with a single point mutation. Previously, it was shown that the reduction potential of the S_2 state in ammonia-treated PSII [40] was at least 2.7 kcal mol^{-1} lower than the reduction potential of the S_2 state in untreated wild-type PSII, and it was proposed to be due to the binding of ammonia to Mn4. Hence, we propose that the higher activation energy for $S_2 \rightarrow S_1$ transition in D1-S169A PSII core complexes arises from a change in the coordination environment of Mn4. These studies thereby further support the

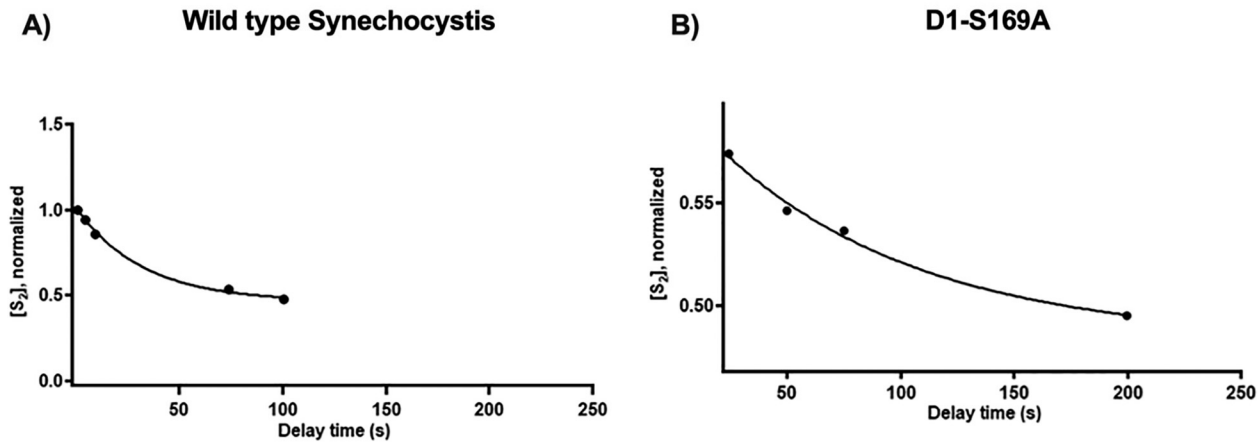

Fig. 3. Comparison of the S_2 decay curves in: A) wild-type and B) D1-S169A PSII core complexes at 15 °C. The decay curves are fit with an exponential decay equation (See Materials and Methods) and the fit parameters are included in Table 1.

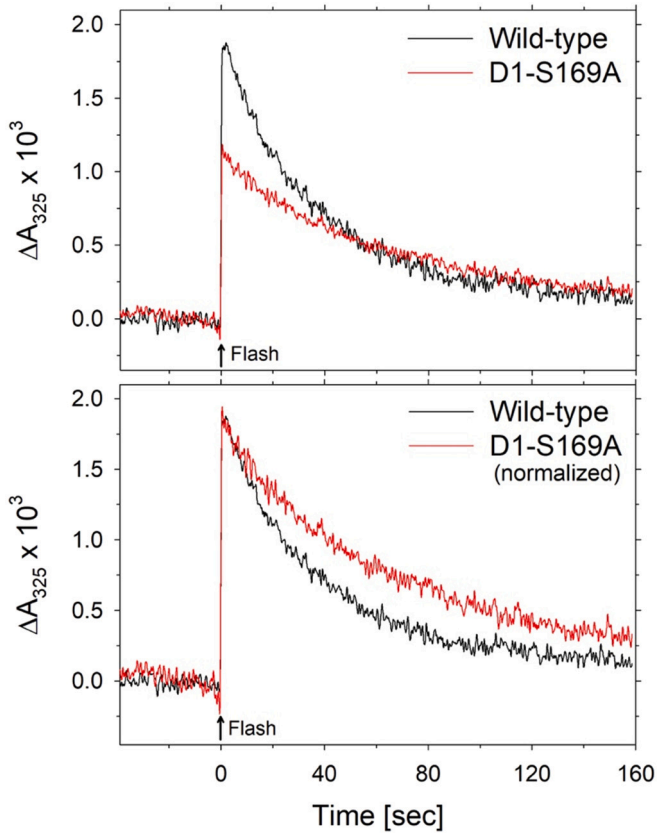

Fig. 4. Formation and decay of $Q_A^{\bullet-}$ after a single flash applied to wild-type (black) and D1-S169A (red) PSII core complexes as measured at 325 nm. For the lower panel, normalization was achieved by multiplying the D1-S169A data by a factor of 1.64. Experimental conditions: 20 μg Chl/mL in 1.2 M betaine, 10% (*v*/v) glycerol, 50 mM MES-NaOH (pH 6.0), 20 mM $CaCl_2$, 5 mM $MgCl_2$, 0.03% *n*-dodecyl-*β*-D-maltoside, 25 μM DCMU, 1% DMSO, 4 °C. The wild-type data represent the average of 72 traces (8 samples). The D1-S169A data represent the average of 144 traces (17 samples).

conclusion that the S_2 state in D1-S169A PSII is structurally distinct from the S_2 state in wild-type PSII, as reflected by the altered S_2-state multiline EPR signal, a reduced rate of S_2 to S_1 state decay and higher activation energy for the $S_2 \rightarrow S_1$ transition. To gain deeper insights into the altered S_2 state, we studied the effect of ammonia treatment on D1-S169A PSII core complexes.

Table 2
$Q_A^{\bullet-}$ decay kinetics in PSII core complexes measured at 325 nm: Comparison of S_2-to-S_1 decay kinetics in wild-type and D1-S169A PSII core complexes, where k_1^{-1} and k_2^{-1} represent the decay rates. Data from Fig. 4 were fit with a bi-phasic exponential decay model.

	k_1		k_2		*constant*
	%	k_1^{-1} (s)	%	k_2^{-1} (s)	%
Wild-type	13 ± 1	7.5 ± 1.0	82 ± 1	38 ± 1	7 ± 1
D1-S169A	13 ± 2	13 ± 2	81 ± 1	76 ± 3	6 ± 1

3.2. Effect of ammonia treatment on D1-S169A PSII

We analyzed the binding of ammonia to the S_2 state of D1-S169A using cw-EPR spectroscopy. After illumination at 200 K and annealing at 258 K, the altered multiline signal observed in D1-S169A [31] was not altered further (Fig. 8). This observation demonstrates that ammonia does not bind to the OEC in D1-S169A PSII core complexes under our experimental conditions. However, we do observe a reduction in the steady-state activity of D1-S169A PSII in the presence of ammonia (Fig. S3). It has been demonstrated that the binding of ammonia to the primary site (Mn4 of the OEC) does not affect the water-oxidation reaction, whereas binding to the secondary-sites does affect the water-oxidation process and reduces the steady-state activity [62–64]. Hence, in D1-S169A PSII, ammonia may bind to the secondary sites of PSII.

3.3. QM/MM calculations on the S_2 state of D1-S169A

We carried out QM/MM calculations on D1-S169A PSII to study the effect of the D1-S169A substitution on the structure of the OEC. QM/MM calculations show that an additional water can bind as a terminal ligand to the Mn4 ion in place of the oxo ligand O5 in the optimized S_2-state structure of D1-S169A PSII (Fig. 9). We refer to this new S_2-state structure as S_2^x. The D1-S169 residue in wild-type PSII is hydrogen bonded to Wx through its side chain. The disruption of the hydrogen bond upon substitution of S169 with A169 increases the Lewis basicity of Wx which then is hypothesized to bind as an additional ligand to the Mn4 ion in place of O5, leading to the observed QM/MM optimized structure. Further QM/MM studies were carried out to confirm that the proposed S_2^x structure is in the low-spin state. This structure is thus consistent with the modified multiline signal centered at g = 2 observed in the EPR spectrum for the S169A PSII (Supplementary Note 1). Additionally, theoretical energetic estimates also suggests the possibility of hindered decay for the novel S_2^x state in D1-S169A PSII (Supplementary Note 1). This is one of the proposed models that is

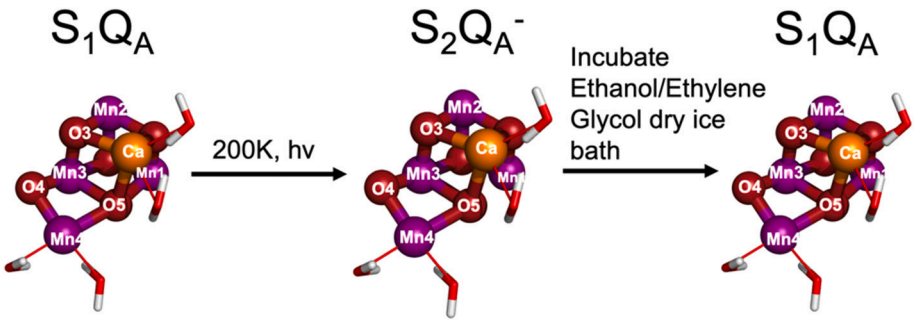

Scheme 1. Generation of the S_2 state followed by its decay kinetics during dark incubation.

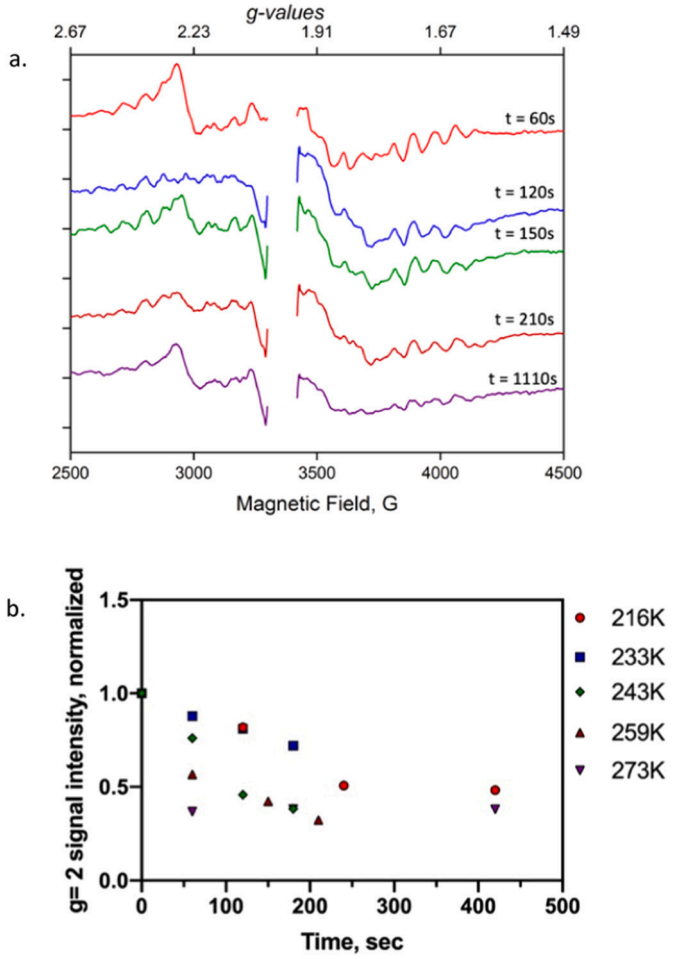

Fig. 5. Kinetics of decay of $S_2Q_A^-$ to S_1Q_A in PSII core complexes isolated from D1-S169A cells. (a) The S_2-state g = 2.0 EPR signal is formed upon illumination at 200 K, as shown in the light − dark spectrum (top red trace). During incubation in darkness at the representative temperature of 259 K in the presence of DCMU, the S_2-state g = 2.0 EPR signal in D1-S169A PSII decreases slower than the S_2-state g = 2.0 EPR signal of wild-type PSII (Fig. S2). (b) Normalized peak-to-peak height of the S_2-state g = 2 EPR signal vs. incubation time at different temperatures.

consistent with the experimental evidence presented in the current study. However, there is strong interconnectivity between the large and the narrow channel, as has been described earlier. Thus, the current proposition does not preclude the delivery of the additional water bonded to Mn4 from the large channel (O1 channel) [65].

4. Discussion

PSII isolated from D1-S169A cells exhibit diminished S-state cycling, perturbations to the FT-IR difference spectra and a slowing of the rate of oxygen release [31]. These features suggest that the D1-S169 residue plays a crucial role in the water-oxidation reaction. Hence, it is important to further elucidate the function of this residue. Elsewhere, we have reported the pH dependence of the steady-state activity and the kinetic solvent isotope effect in both wild-type and D1-S169A PSII. The observed KSIE value of D1-S169A PSII around the optimal pH is 1.61 ± 0.04, which is in good agreement with that of wild-type PSII (1.48 ± 0.07) [66]. This value reflects the effect of H/D exchange on the rate-determining step. Previous studies reveal that an alteration in the proton-transfer mechanism results in a change of the KSIE values by ~1.0 unit [66]. Hence, the similarity in the KSIE values of wild-type and D1-S169A PSII indicates that the proton-transfer mechanism is not significantly affected by the A169 substitution. Further, the proton inventory curves at pL 6.5 are also similar in both wild-type and D1-S169A PSII [66]. Bicarbonate is known to recover the damaged activity in D2-K317A mutated PSII, which is known to affect the proton-transfer pathway [67]. However, bicarbonate fails to rescue the damaged PSII in D1-S169A (Fig. S4). These studies provide strong evidence that the proton-transfer process in D1-S169A PSII is not significantly perturbed despite the mutation-induced alterations to the H-bond networks [31]. How then to explain the damped S-state cycling, slowed oxygen release, and the higher activation energy of the S_2 to S_1 state transition in D1-S169A PSII core complexes?

The low-spin isomer of the S_2 state is characterized by an EPR spectrum that shows 20–22 characteristic hyperfine lines centered at g = 2. In D1-S169A PSII, the hyperfine spacing of this multiline signal is decreased, but is not decreased further by the addition of ammonia, even after annealing at 258 K. In contrast, the similarly decreased hyperfine spacing of the S_2-state multiline EPR signal in D1-D61A PSII is decreased further by ammonia and no annealing step is needed [28]. On the basis of pulsed ^{55}Mn ENDOR studies, the similar alterations to the S_2-state multline EPR signal observed previously in ammonia-treated [27–30], Ca-depleted [54,55] and Sr/Ca substituted wild-type PSII [39,56–58] have been attributed to subtle changes in the environment of the S_2 state's single Mn(III) ion, caused in turn by modest alterations to the magnetic couplings between the individual Mn ions [55,58,68–70]. The similar alterations to the S_2-state multiline EPR signal caused by the D1-D61A mutation were attributed to similar alterations to the magnetic couplings caused by perturbation of hydrogen bonds by the D1-D61A mutation [28]. As pointed out previously [31], the alterations to the S_2-state multline EPR signal caused by the D1-S169A mutation may have the same origin. Because ammonia alters the multline signal in D1-D61A PSII without need for an annealing step, it was suggested that the energetic barrier for binding ammonia to Mn4 is decreased by the perturbations of hydrogen bonds caused by the D1-D61A mutation [28]. One possibility is that the perturbations to the same network of hydrogen bonds caused by the D1-S169A mutation

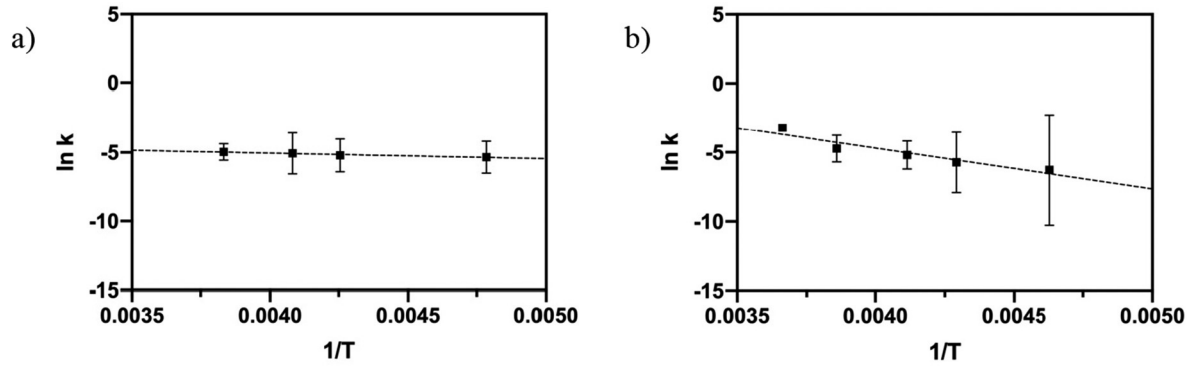

Fig. 6. Arrhenius analysis of the decay kinetics of $S_2Q_A^-$ to S_1Q_A. a) wild-type *Synechocystis* PSII, E_a = 0.80 ± 0.13 kcal mol^{-1}. b) D1-S169A PSII, E_a = 5.87 ± 1.15 kcal mol^{-1}.

increases the energetic barrier for binding ammonia to Mn4. Another possibility is suggested by our QM/MM S_2^x state structure of D1-S169A PSII that shows the presence of an additional water ligand to Mn4 in place of the O5 oxo ligand. These structural changes may both alter the S_2-state multiline EPR signal and increase the activation barrier for binding ammonia to Mn4 due to the presence of a coordinatively saturated Mn4. In addition, the binding of an additional water molecule to Mn4 in place of O5 may increase the activation energy for the S_2 to S_1 transition and thereby slow the decay of the S_2^x state. The additional stability of the S_2^x state observed here is in good agreement with the decrease in redox potential (S_2/S_1) observed for S169A cells [71]. This additional water may arise from the narrow channel, as D1-S169 is hydrogen bonded to the waters in this channel. However, the strong inter-connected hydrogen-bonding network between the channels can also lead to the bonding of a large-channel water to the Mn4 of the OEC [72,73]. Another possible explanation of the increased stability of the S_2^x state is suggested by a recent multi-conformer continuum electrostatics (MCCE) study of the relative stabilties of the two isomers of the S_2 state [74]. On the basis of these calculations, the transition from the S_1 state to the low-spin isomer of the S_2 state (the form that exhibits the multiline EPR signal) proceeds with partial deprotonation of W2, with the fractional proton ending up on D1-D61, D1-E329, and possiblity elsewhere in the extensive network of hydrogen bonds that surround the Mn_4CaO_5 cluster. Alterations to these networks caused by the S169A mutation (or by the binding of ammonia) might alter the equilibrium between the S_2Y_Z and $S_1Y_Z^{\bullet}$ states, to stabilize the S_2 state, thereby slowing the S_2-decay kinetics. Finally, because our studies show that the S_2^x state is thermodynamically less favorable (due to a higher activation energy) to decay back to the S_1 state compared to the native S_2 state, this state is more favorably poised to proceed to the S_3 state via transfer of a water to Mn1 after the formation of the S_2^x state [72]. Hence, this novel S_2 state (S_2^x) of D1-S169A may mimic the intermediate state formed during the S_2 to S_3 transition and provide new insights into the mechanism of substrate-water delivery to the OEC.

5. Conclusions

Our analysis of D1-S169A PSII highlights that the S_2 state in the mutated PSII is structurally altered, thermodynamically more stable and remains unperturbed upon ammonia treatment. Additional experiments probing the S_2^x-state structure using pulsed EPR experiments will help in identifying the detailed structural changes of the S_2 state. Finally, it will be interesting to probe the S_3-state formation in D1-S169A PSII to elucidate the effects of this mutation on the mechanistic details of the S_2 to S_3 transition.

Abbreviations

Chl	chlorophyll
D1	D1 polypeptide of PSII
D2	D2 polypeptide of PSII
DCBQ	2,6-dichloro-*p*-benzoquinone

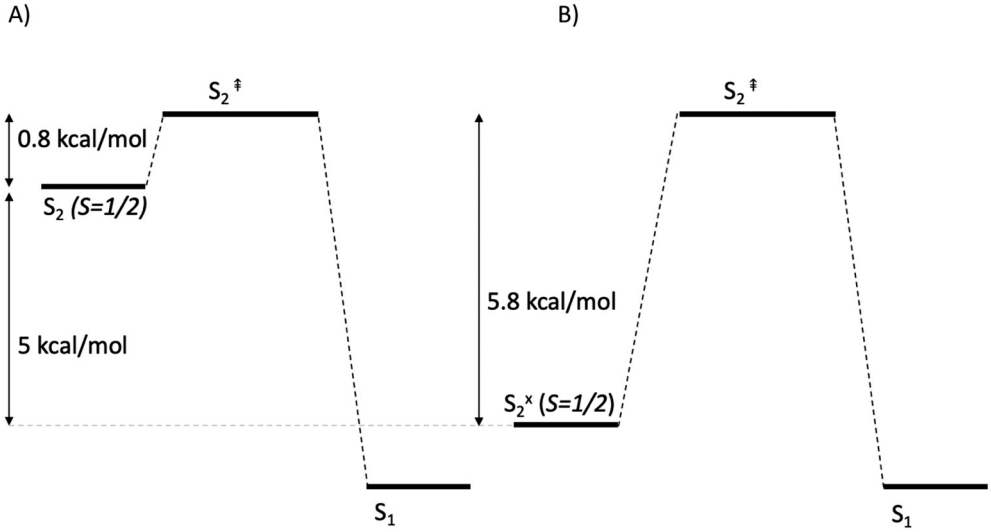

Fig. 7. Energetics scheme for the decay of the $S_2Q_A^-$ state to the S_1Q_A state. A) wild-type *Synechocystis* PSII. B) D1-S169A PSII. The double dagger symbol denotes a transition state.

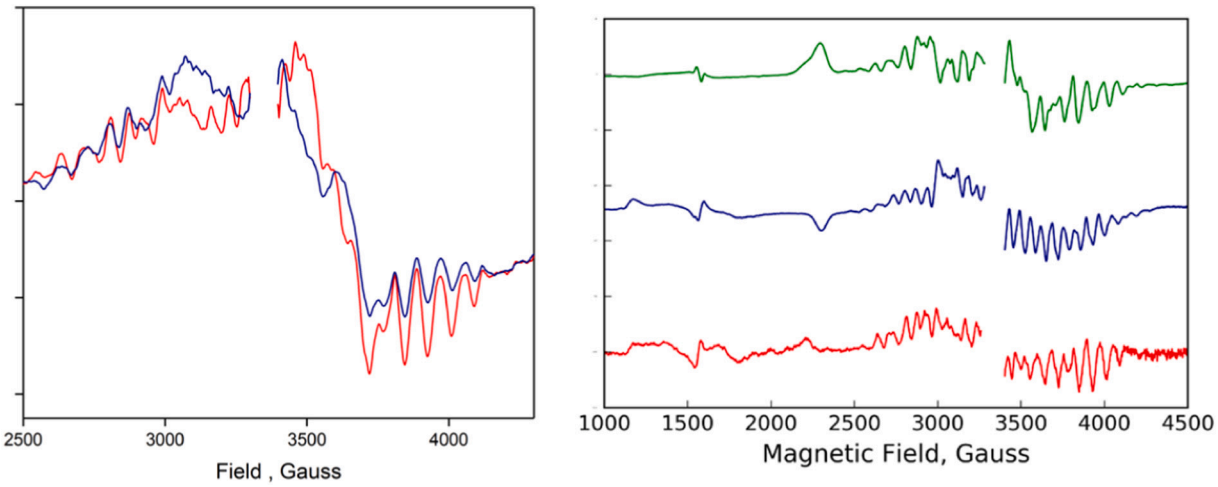

Fig. 8. Left panel: Comparison of the difference EPR spectra of the ammonia-treated D1-S169A PSII core complexes. The red trace corresponds to the difference between the S_2 and S_1 states. The blue trace corresponds to the difference between the annealed-S_2 and S_1 states. The S_2 state was generated by illuminating the PSII sample at 200 K. The annealed-S_2 state was generated by warming the PSII sample to 258 K for 1 min in the dark, after generating the S_2 state. Right panel: Comparison of the EPR spectra of the S_2 state of wild-type PSII core complexes (green), wild-type PSII core complexes treated with ammonia (blue) and D1-S169A PSII core complexes (red) (Adapted from [28]).

EPR	electron paramagnetic resonance
FTIR	Fourier transform infrared
OEC	oxygen-evolving complex
Pheo	Pheophytin
PPBQ	2-phenyl-1,4-benzoquinone
PSII	photosystem II
Y_Z	tyrosine Z

Author contributions

The manuscript was written through contributions of all authors. All authors have given approval to the final version of the manuscript.

Declaration of competing interest

The authors declare that they have no known competing financial interests or personal relationships that could have appeared to influence the work reported in this paper.

Acknowledgement

This work was supported by grants from the Department of Energy, Office of Basic Energy Sciences, Division of Chemical Sciences. Oxygen-release and EPR studies were supported by Grant DE-FG02-05ER15646 (to G.W.B.). Mutant construction and time-resolved optical absorption measurements were supported by Grant DE-SC0005291 (to R.J.D.). Computational studies were supported by the DOE Grant DE-SC0001423 (to V.S.B) and supercomputer time from NERSC.

Appendix A. Supplementary data

Supplementary data to this article can be found online at https://

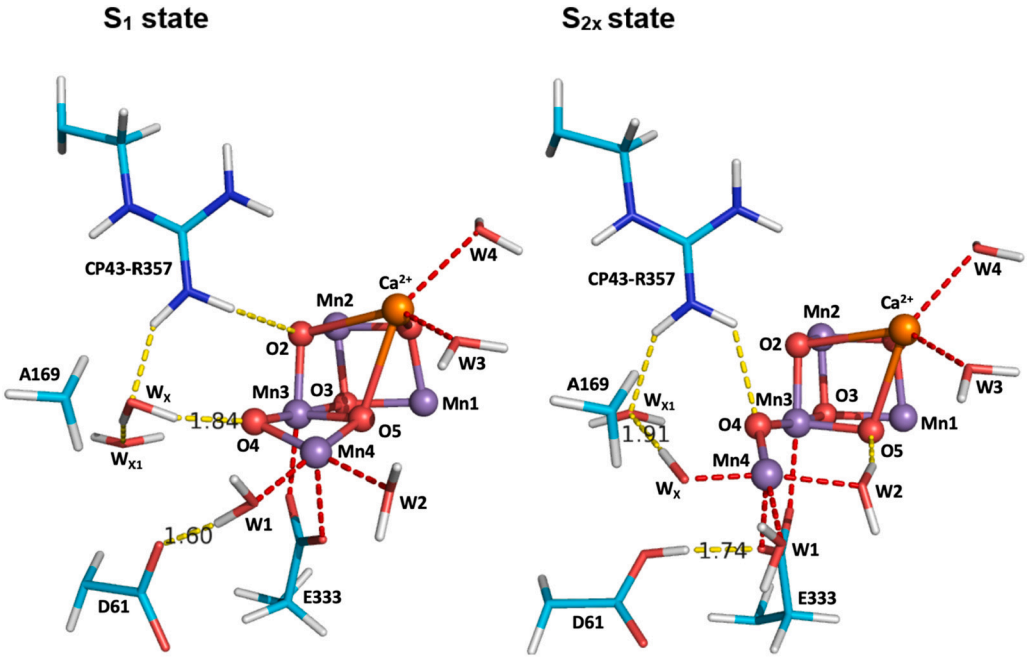

Fig. 9. The QM/MM optimized S_1 structure and S_2^x structure of D1-S169A PSII. In the S_1 structure, we observe that D1-S169A is not hydrogen bonded to Wx. In S_2^x structure, we observe that Wx is deprotonated and is bound to Mn4. When D61 accepts the proton from Wx, it shifts to form a new hydrogen bond with E333. The Mn ions are marked in purple, O in red, and Ca in orange.

doi.org/10.1016/j.bbabio.2020.148301.

References

[1] J.D. Blakemore, R.H. Crabtree, G.W. Brudvig, Molecular catalysts for water oxidation, Chem. Rev. 115 (2015) 12974–13005.

[2] H.-L. Huang, I. Ghosh, G. Banerjee, G.W. Brudvig, Progress towards unraveling the water-oxidation mechanism of photosystem II, in: James Barber, Alexander V. Ruban, Peter J. Nixon (Eds.), Oxygen Production and Reduction in Artificial and Natural Systems, World Scientific, Singapore, 2019, pp. 285–306.

[3] D. Pantazis, Missing pieces in the puzzle of biological water oxidation, ACS Catal. 8 (2018) 9477–9507.

[4] M. Perez-Navarro, F. Neese, W. Lubitz, D.A. Pantazis, N. Cox, Recent developments in biological water oxidation, Curr. Opin. Chem. Biol. 31 (2016) 113–119.

[5] D.J. Vinyard, G.W. Brudvig, Progress toward a molecular mechanism of water oxidation in photosystem II, Annu. Rev. Phys. Chem. 68 (2017) 101–116.

[6] L. Vogt, D.J. Vinyard, S. Khan, G.W. Brudvig, Oxygen-evolving complex of photosystem II: an analysis of second-shell residues and hydrogen-bonding networks, Curr. Opin. Chem. Biol. 25 (2015) 152–158.

[7] B. Kok, B. Forbush, M. McGloin, Cooperation of charges in photosynthetic O_2 evolution-I. A linear four step mechanism, Photochem. Photobiol., 11 (1970) 457–475.

[8] H. Dau, M. Haumann, Eight steps preceding O–O bond formation in oxygenic photosynthesis—a basic reaction cycle of the photosystem II manganese complex, Biochim. Biophys. Acta 1767 (2007) 472–483.

[9] F. Müh, A. Zouni, The nonheme iron in photosystem II, Photosynth. Res. 116 (2013) 295–314.

[10] F. Müh, C. Glöckner, J. Hellmich, A. Zouni, Light-induced quinone reduction in photosystem II, Biochim. Biophys. Acta 1817 (2012) 44–65.

[11] D. Shevela, J.J. Eaton-Rye, J.R. Shen, Photosystem II and the unique role of bicarbonate: a historical perspective, Biochim. Biophys. Acta 1817 (2012) 1134–1151.

[12] K. Saito, A.W. Rutherford, H. Ishikita, Mechanism of tyrosine D oxidation in photosystem II, Proc. Natl. Acad. Sci. U. S. A. 110 (2013) 7690–7695.

[13] M. Suga, F. Akita, K. Hirata, G. Ueno, H. Murakami, Y. Nakajima, T. Shimizu, K. Yamashita, M. Yamamoto, H. Ago, Native structure of photosystem II at 1.95 Å resolution viewed by femtosecond X-ray pulses, Nature 517 (2015) 99–103.

[14] J. Kern, R. Chatterjee, I.D. Young, F.D. Fuller, L. Lassalle, M. Ibrahim, S. Gul, T. Fransson, A.S. Brewster, R. Alonso-Mori, Structures of the intermediates of Kok's photosynthetic water oxidation clock, Nature 563 (2018) 421–425.

[15] R. Pal, C.F. Negre, L. Vogt, R. Pokhrel, M.Z. Ertem, G.W. Brudvig, V.S. Batista, S_0-state model of the oxygen-evolving complex of photosystem II, Biochemistry 52 (2013) 7703–7706.

[16] Y. Umena, K. Kawakami, J.-R. Shen, N. Kamiya, Crystal structure of oxygen-evolving photosystem II at a resolution of 1.9 Å, Nature 473 (2011) 55–60.

[17] M. Suga, F. Akita, M. Sugahara, M. Kubo, Y. Nakajima, T. Nakane, K. Yamashita, Y. Umena, M. Nakabayashi, T. Yamane, Light-induced structural changes and the site of O = O bond formation in PSII caught by XFEL, Nature 543 (2017) 131–135.

[18] D.A. Pantazis, W. Ames, N. Cox, W. Lubitz, F. Neese, Two interconvertible structures that explain the spectroscopic properties of the oxygen-evolving complex of photosystem II in the S_2 state, Angew. Chem. Int. Ed. 51 (2012) 9935–9940.

[19] R. Pokhrel, G.W. Brudvig, Oxygen-evolving complex of photosystem II: correlating structure with spectroscopy, Phys. Chem. Chem. Phys. 16 (2014) 11812–11821.

[20] N. Cox, M. Retegan, F. Neese, D.A. Pantazis, A. Boussac, W. Lubitz, Electronic structure of the oxygen-evolving complex in photosystem II prior to OO bond formation, Science 345 (2014) 804–808.

[21] W. Hillier, T. Wydrzynski, ^{18}O-water exchange in photosystem II: substrate binding and intermediates of the water splitting cycle, Coord. Chem. Rev. 252 (2008) 306–317.

[22] H. Nilsson, F. Rappaport, A. Boussac, J. Messinger, Substrate–water exchange in photosystem II is arrested before dioxygen formation, Nat. Commun. 5 (2014) 4305.

[23] M. Retegan, D.A. Pantazis, Interaction of methanol with the oxygen-evolving complex: atomistic models, channel identification, species dependence, and mechanistic implications, Chem. Sci. 7 (2016) 6463–6476.

[24] P.H. Oyala, T.A. Stich, J.A. Stull, F. Yu, V.L. Pecoraro, R.D. Britt, Pulse electron paramagnetic resonance studies of the interaction of methanol with the S_2 state of the Mn_4O_5Ca cluster of photosystem II, Biochemistry 53 (2014) 7914–7928.

[25] H. Nagashima, H. Mino, Location of methanol on the S_2 state Mn cluster in photosystem II studied by proton matrix electron nuclear double resonance, J. Phys. Chem. Lett. 8 (2017) 621–625.

[26] H. Yata, T. Noguchi, Mechanism of methanol inhibition of photosynthetic water oxidation as studied by Fourier transform infrared difference and time-resolved infrared spectroscopies, Biochemistry 57 (2018) 4803–4815.

[27] D.A. Marchiori, P.H. Oyala, R.J. Debus, T.A. Stich, R.D. Britt, Structural effects of ammonia binding to the Mn_4CaO_5 cluster of photosystem II, J. Phys. Chem. B 122 (2018) 1588–1599.

[28] P.H. Oyala, T.A. Stich, R.J. Debus, R.D. Britt, Ammonia binds to the dangler manganese of the photosystem II oxygen-evolving complex, J. Am. Chem. Soc. 137 (2015) 8829–8837.

[29] M. Pérez Navarro, W.M. Ames, H. Nilsson, T. Lohmiller, D.A. Pantazis, L. Rapatskiy, M.M. Nowaczyk, F. Neese, A. Boussac, J. Messinger, Ammonia binding to the oxygen-evolving complex of photosystem II identifies the solvent-exchangeable oxygen bridge (μ-oxo) of the manganese tetramer, Proc. Natl. Acad. Sci. U. S. A. 110 (2013) 15561–15566.

[30] W.F. Beck, J.C. de Paula, G.W. Brudvig, Ammonia binds to the manganese site of the oxygen-evolving complex of photosystem II in the S_2 state, J. Am. Chem. Soc. 108 (1986) 4018–4022.

[31] I. Ghosh, G. Banerjee, C.J. Kim, K. Reiss, V.S. Batista, R.J. Debus, G.W. Brudvig, D1-S169A substitution of photosystem II perturbs water oxidation, Biochemistry 58 (2019) 1379–1387.

[32] P.L. Dilbeck, H. Bao, C.L. Neveu, R.L. Burnap, Perturbing the water cavity surrounding the manganese cluster by mutating the residue D1-valine 185 has a strong effect on the water oxidation mechanism of photosystem II, Biochemistry 52 (2013) 6824–6833.

[33] C.J. Kim, H. Bao, R.L. Burnap, R. Debus, Impact of D1-V185 on the water molecules that facilitate O_2 formation by the catalytic Mn_4CaO_5 cluster in photosystem II, Biochemistry 57 (2018) 4299–4311.

[34] M. Sugiura, T. Tibiletti, I. Takachi, Y. Hara, S. Kanawaku, J. Sellés, A. Boussac, Probing the role of Valine 185 of the D1 protein in the photosystem II oxygen evolution, Biochim. Biophys. Acta 1859 (2018) 1259–1273.

[35] G. Banerjee, I. Ghosh, C.J. Kim, R.J. Debus, G.W. Brudvig, Substitution of the D1-Asn87 site in photosystem II of cyanobacteria mimics the chloride-binding characteristics of spinach photosystem II, J. Biol. Chem. 293 (2018) 2487–2497.

[36] A. Yamasato, T. Kamada, K. Satoh, The random mutational analysis of the structure and function of photosystem II reaction center targeting to the psbAII gene of *Synechocystis* sp. PCC 6803, Science Access, 3 (2001).

[37] H. Suzuki, J. Yu, T. Kobayashi, H. Nakanishi, P.J. Nixon, T. Noguchi, Functional roles of D2-Lys317 and the interacting chloride ion in the water oxidation reaction of photosystem II as revealed by Fourier transform infrared analysis, Biochemistry 52 (2013) 4748–4757.

[38] H.-A. Chu, R.J. Debus, G.T. Babcock, D1-Asp170 is structurally coupled to the oxygen evolving complex in photosystem II as revealed by light-induced fourier transform infrared difference spectroscopy, Biochemistry 40 (2001) 2312–2316.

[39] M.A. Strickler, L.M. Walker, W. Hillier, R.J. Debus, Evidence from biosynthetically incorporated strontium and FTIR difference spectroscopy that the C-terminus of the D1 polypeptide of photosystem II does not ligate calcium, Biochemistry 44 (2005) 8571–8577.

[40] D.J. Vinyard, G.W. Brudvig, Insights into substrate binding to the oxygen-evolving complex of photosystem II from ammonia inhibition studies, Biochemistry 54 (2015) 622–628.

[41] D.J. Vinyard, C.E. Zachary, G. Ananyev, G.C. Dismukes, Thermodynamically accurate modeling of the catalytic cycle of photosynthetic oxygen evolution: a mathematical solution to asymmetric Markov chains, Biochim. Biophys. Acta 1827 (2013) 861–868.

[42] R.J. Debus, K.A. Campbell, J.M. Peloquin, D.P. Pham, R.D. Britt, Histidine 332 of the D1 polypeptide modulates the magnetic and redox properties of the manganese cluster and tyrosine Y_Z in photosystem II, Biochemistry 39 (2000) 470–478.

[43] R.J. Debus, K.A. Campbell, D.P. Pham, A.-M.A. Hays, R.D. Britt, Glutamate 189 of the D1 polypeptide modulates the magnetic and redox properties of the manganese cluster and tyrosine Y_Z in photosystem II, Biochemistry 39 (2000) 6275–6287.

[44] M. Askerka, G.W. Brudvig, V.S. Batista, The O_2-evolving complex of photosystem II: recent insights from quantum mechanics/molecular mechanics (QM/MM), extended X-ray absorption fine structure (EXAFS), and femtosecond X-ray crystallography data, Acc. Chem. Res. 50 (2016) 41–48.

[45] T. Vreven, K. Morokuma, The ONIOM (our own N-layered integrated molecular orbital + molecular mechanics) method for the first singlet excited (S_1) state photoisomerization path of a retinal protonated Schiff base, J. Chem. Phys. 113 (2000) 2969–2975.

[46] M. J. Frisch, G. W. Trucks, H. B. Schlegel, G. E. Scuseria, M. A. Robb, J. R. Cheeseman, G. Scalmani, V. Barone, G. A. Petersson, H. Nakatsuji, X. Li, M. Caricato, A. V. Marenich, J. Bloino, B. G. Janesko, R. Gomperts, B. Mennucci, H. P. Hratchian, J. V. Ortiz, A. F. Izmaylov, J. L. Sonnenberg, D. Williams-Young, F. Ding, F. Lipparini, F. Egidi, J. Goings, B. Peng, A. Petrone, T. Henderson, D. Ranasinghe, V. G. Zakrzewski, J. Gao, N. Rega, G. Zheng, W. Liang, M. Hada, M. Ehara, K. Toyota, R. Fukuda, J. Hasegawa, M. Ishida, T. Nakajima, Y. Honda, O. Kitao, H. Nakai, T. Vreven, K. Throssell, J. A. Montgomery, Jr., J. E. Peralta, F. Ogliaro, M. J. Bearpark, J. J. Heyd, E. N. Brothers, K. N. Kudin, V. N. Staroverov, T. A. Keith, R. Kobayashi, J. Normand, K. Raghavachari, A. P. Rendell, J. C. Burant, S. S. Iyengar, J. Tomasi, M. Cossi, J. M. Millam, M. Klene, C. Adamo, R. Cammi, J. W. Ochterski, R. L. Martin, K. Morokuma, O. Farkas, J. B. Foresman, and D. J. Fox, Gaussian 16, Revision C.01, Gaussian, Inc., Wallingford CT, 2016.

[47] M. Askerka, J. Wang, G.W. Brudvig, V.S. Batista, Structural changes in the oxygen-evolving complex of photosystem II induced by the S_1 to S_2 transition: a combined XRD and QM/MM study, Biochemistry 53 (2014) 6860–6862.

[48] A.D. Becke, Density-functional exchange-energy approximation with correct asymptotic behavior, Phys. Rev. A 38 (1988) 3098.

[49] A.D. Becke, Density-functional thermochemistry. III. The role of exact exchange, J. Chem. Phys., 98 (1993) 5648–5652.

[50] P.J. Hay, W.R. Wadt, Ab initio effective core potentials for molecular calculations. Potentials for K to Au including the outermost core orbitals, J. Chem. Phys., 82 (1985) 299–310.

[51] D.A. da Silva Filho, V. Coropceanu, D. Fichou, N.E. Gruhn, T.G. Bill, J. Gierschner, J. Cornil, J.-L. Brédas, Hole-vibronic coupling in oligothiophenes: impact of backbone torsional flexibility on relaxation energies, Philos. Trans. Royal Soc. A 365 (2007) 1435–1452.

[52] P.C. Hariharan, J.A. Pople, The influence of polarization functions on molecular orbital hydrogenation energies, Theor. Chim. Acta 28 (1973) 213–222.

[53] D. Case, T. Darden, T. Cheatham III, C. Simmerling, J. Wang, R. Duke, R. Luo, R. Walker, W. Zhang, K. Merz, AMBER 12, University of California: San Francisco 2012 (2010) 1–826.

[54] A. Boussac, J.L. Zimmermann, A.W. Rutherford, EPR signals from modified charge accumulation states of the oxygen-evolving enzyme in calcium-deficient photosystem II, Biochemistry 28 (1989) 8984–8989.
[55] T. Lohmiller, N. Cox, J.-H. Su, J. Messinger, W.J. Lubitz, The basic properties of the electronic structure of the oxygen-evolving complex of photosystem II are not perturbed by Ca^{2+} removal, J. Biol. Chem. 287 (2012) 24721–24733.
[56] G. Chen, G. Han, E. Göransson, F. Mamedov, S.R. Styring, Stability of the S_3 and S_2 state intermediates in photosystem II directly probed by EPR spectroscopy, Biochemistry 51 (2011) 138–148.
[57] S.A. Styring, A.W. Rutherford, The microwave power saturation of SII_{slow} varies with the redox state of the oxygen-evolving complex in photosystem II, Biochemistry 27 (1988) 4915–4923.
[58] N. Cox, L. Rapatskiy, J.-H. Su, D.A. Pantazis, M. Sugiura, L. Kulik, P. Dorlet, A.W. Rutherford, F. Neese, A. Boussac, Effect of Ca^{2+}/Sr^{2+} substitution on the electronic structure of the oxygen-evolving complex of photosystem II: a combined multifrequency EPR, ^{55}Mn-ENDOR, and DFT study of the S_2 state, J. Am. Chem. Soc. 133 (2011) 3635–3648.
[59] S. Styring, A.W. Rutherford, Deactivation kinetics and temperature dependence of the S-state transitions in the oxygen-evolving system of photosystem II measured by EPR spectroscopy, Biochim. Biophys. Acta 933 (1988) 378–387.
[60] H.-A. Chu, A.P. Nguyen, R.J. Debus, Site-directed photosystem II mutants with perturbed oxygen-evolving properties. 1. Instability or inefficient assembly of the manganese cluster *in vivo*, Biochemistry 33 (1994) 6137–6149.
[61] J.G. Metz, P.J. Nixon, M. Rogner, G.W. Brudvig, B.A. Diner, Directed alteration of the D1 polypeptide of photosystem II: evidence that tyrosine-161 is the redox component, Z, connecting the oxygen-evolving complex to the primary electron donor, P_{680}, Biochemistry 28 (1989) 6960–6969.
[62] A. Boussac, A.W. Rutherford, S. Styring, Interaction of ammonia with the water splitting enzyme of photosystem II, Biochemistry 29 (1990) 24–32.
[63] N. Schuth, Z. Liang, M. Schonborn, A. Kussicke, R. Assuncao, I. Zaharieva, Y. Zilliges, H. Dau, Inhibitory and non-inhibitory NH_3 binding at the water-oxidizing manganese complex of photosystem II suggests possible sites and a rearrangement mode of substrate water molecules, Biochemistry 56 (2017) 6240–6256.
[64] W.F. Beck, G.W. Brudvig, Binding of amines to the oxygen-evolving center of photosystem II, Biochemistry 25 (1986) 6479–6486.
[65] M. Suga, F. Akita, K. Yamashita, Y. Nakajima, G. Ueno, H. Li, T. Yamane, K. Hirata, Y. Umena, S. Yonekura, An oxyl/oxo mechanism for oxygen-oxygen coupling in PSII revealed by an x-ray free-electron laser, Science 366 (2019) 334–338.
[66] I. Ghosh, S. Khan, G. Banerjee, A. Dziarsky, D. Vinyard, R.J. Debus, G.W. Brudvig, Insights on proton-transfer pathways during water oxidation in photosystem II, J. Phys. Chem. B 123 (2019) 8195–8202.
[67] G. Banerjee, I. Ghosh, C.J. Kim, R.J. Debus, G.W. Brudvig, Bicarbonate rescues damaged proton-transfer pathway in photosystem II, Biochim. Biophys. Acta 8 (2019) 611–617.
[68] T.A. Stich, G.J. Yeagle, R.J. Service, R.J. Debus, R.D. Britt, Ligation of D1-His332 and D1-Asp170 to the manganese cluster of photosystem II from *Synechocystis* assessed by multifrequency pulse EPR spectroscopy, Biochemistry 50 (2011) 7390–7404.
[69] T. Lohmiller, V. Krewald, M.P. Navarro, M. Retegan, L. Rapatskiy, M.M. Nowaczyk, A. Boussac, F. Neese, W. Lubitz, D.A. Pantazis, Structure, ligands and substrate coordination of the oxygen-evolving complex of photosystem II in the S_2 state: a combined EPR and DFT study, Phys. Chem. Chem. Phys. 16 (2014) 11877–11892.
[70] D.A. Marchiori, P.H. Oyala, R.J. Debus, T.A. Stich, R.D. Britt, Structural effects of ammonia binding to the Mn_4CaO_5 cluster of photosystem II, J. Phys. Chem. B 122 (2018) 1588–1599.
[71] Y. Shimada, T. Kitajima-Ihara, R. Nagao, T. Noguchi, Role of the O4 channel in photosynthetic water oxidation as revealed by fourier transform infrared difference and time-resolved infrared analysis of the D1-S169A mutant, J. Phys. Chem.B 124 (2020) 1470–1480.
[72] M. Amin, D. Kaur, K. Yang, J. Wang, Z. Mohamed, G. Brudvig, M. Gunner, V.S. Batista, Thermodynamics of the S_2-to-S_3 state transition of the oxygen-evolving complex of photosystem II, Phys. Chem. Chem. Phys. 21 (2019) 20840–20848.
[73] C.J. Kim, R.J. Debus, One of the substrate waters for O_2 formation in photosystem II is provided by the water-splitting Mn_4CaO_5 cluster's Ca^{2+} ion, Biochemistry 58 (2019) 3185–3192.
[74] D. Kaur, W. Szejgis, J. Mao, M. Amin, K.M. Reiss, M. Askerka, X. Cai, U. Khaniya, Y. Zhang, G.W. Brudvig, Relative stability of the S_2 isomers of the oxygen evolving complex of photosystem II, Photosynth. Res. 141 (2019) 1–11.
[75] X.-S. Tang, B.A. Diner, Biochemical and spectroscopic characterization of a new oxygen-evolving photosystem I1 core complex from the cyanobacterium *Synechocystis* PCC 6803, Biochemistry 33 (1994) 4594–4603.